

Excitonic emissions and above-band-gap luminescence in the single-crystal perovskite semiconductors CsPbBr₃ and CsPbCl₃

M. Sebastian,¹ J. A. Peters,¹ C. C. Stoumpos,² J. Im,³ S. S. Kostina,¹ Z. Liu,¹ M. G. Kanatzidis,²
A. J. Freeman,³ and B. W. Wessels¹

¹*Department of Material Science and Engineering, Northwestern University, Evanston, Illinois 60208, USA*

²*Department of Chemistry, Northwestern University, Evanston, Illinois 60208, USA*

³*Department of Physics and Astronomy, Northwestern University, Evanston, Illinois 60208, USA*

(Received 1 May 2015; revised manuscript received 14 September 2015; published 29 December 2015)

The ternary compounds CsPbX₃ ($X = \text{Br}$ or Cl) have perovskite structures that are being considered for optical and electronic applications such as lasing and gamma-ray detection. An above-band-gap excitonic photoluminescence (PL) band is seen in both CsPbX₃ compounds. An excitonic emission peak centered at 2.98 eV, ~ 0.1 eV above the room-temperature band gap, is observed for CsPbCl₃. The thermal quenching of the excitonic luminescence is well described by a two-step quenching model, yielding activation energies of 0.057 and 0.0076 eV for high- and low-temperature regimes, respectively. CsPbBr₃ exhibits bound excitonic luminescence peaks located at 2.29 and 2.33 eV that are attributed to recombination involving Br vacancy centers. Activation energies for thermal quenching of the excitonic luminescence of 0.017 and 0.0007 eV were calculated for CsPbBr₃. Temperature-dependent PL experiments reveal unexpected blueshifts for all excitonic emission peaks in CsPbX₃ compounds. A phonon-assisted step-up process leads to the blueshift in CsPbBr₃ emission, while there is a contribution from band-gap widening in CsPbCl₃. The absence of significant deep level defect luminescence in these compounds makes them attractive candidates for high-resolution, room-temperature radiation detection.

DOI: [10.1103/PhysRevB.92.235210](https://doi.org/10.1103/PhysRevB.92.235210)

PACS number(s): 78.55.Fv, 71.35.-y, 07.85.Fv, 61.72.S-

I. INTRODUCTION

The last few years have witnessed a dramatic increase of research on the halide perovskite compounds of group IV metal ions. This long-known class of semiconductors has been studied starting as far back as the 1950s, mainly through the pioneering work of Moller on the CsPbX₃ compound ($X = \text{Cl}$, Br , I) [1,2]. Since then, these perovskite compounds have attracted much attention due to their remarkable optical [3–6] and electronic [7] properties and the numerous temperature-induced structural phase transitions [8]. The discovery that ignited the recent explosive growth in the field was the realization of efficient dye-sensitized solar cells (DSSCs) using perovskite structure CH₃NH₃PbI₃ as the light-absorbing component, thus achieving a 4% conversion efficiency [9]. After the initial discovery, the liquid electrolyte was eliminated in favor of an all-solid state photovoltaic device, marked by the successful employment of CsSnI₃ [10] and CH₃NH₃PbI₃-based perovskites [11] as hole transport and light-absorber components, respectively. Currently, the perovskite solar cells are able to deliver conversion efficiencies of $\sim 20\%$ [12], clearly demonstrating the excellent photoconducting properties of the halide perovskite semiconductors. However, aside from the initial reports on photoconductivity of the CsPbX₃ compounds [1] only a few experiments dealt with the charge-transport properties of these compounds and in most of them the measured electrical properties were attributed to ionic motion [13]. We recently focused our attention on the development of CsPbX₃ [14,15] and other halide semiconductor compounds [16] to utilize their photoconversion potential in the field of high-energy radiation detection.

Gamma-ray spectroscopy is widely used in fields such as security, medicine, and astrophysics. For many of these applications, it is important to have materials that are able to detect gamma rays with high-energy resolution at room temperature.

This can be achieved by using semiconductors that have a large band gap, high density, and optimal charge-transport properties as given by the mobility-lifetime ($\mu\tau$) product. Current detector materials are semi-insulating semiconductors containing heavy elements, such as Cd_{0.9}Zn_{0.1}Te (CZT) and TlBr [17]. These semiconductors have high resistivities ($> 10^9 \Omega \text{ cm}$) that result in low detector background noise, leading to high-resolution gamma-ray spectra. In addition the semiconductor CZT has a $\mu\tau$ value on the order of $10^{-2} \text{ cm}^2 \text{ V}^{-1}$ and TlBr on the order of $10^{-3} \text{ cm}^2 \text{ V}^{-1}$. There are, however, several drawbacks associated with these two compounds. CZT is known to exhibit twinning and Te precipitation formation that lowers the $\mu\tau$ value, whereas TlBr is mechanically soft and thus deleterious line defects are readily formed. In addition, TlBr suffers from electric polarization over time [17,18], which results in a built-in field that impedes current flow in the material, causing a decrease in detector performance over time. These effects limit the detector efficiency and its spectral resolution.

As a result, other compounds such as the ternary compounds CsPbX₃ ($X = \text{Br}$, Cl) are being considered as room-temperature x-ray and gamma-ray detector materials due to their high density, high resistivity, $\mu\tau$, and wide band gap [14,15]. Large single crystals of these compounds were grown via a modified Bridgman technique. They have direct band gaps and high $\mu\tau$ values on the order of $10^{-3} \text{ cm}^2 \text{ V}^{-1}$ for both electrons and holes stemming from the favorable electronic structure of the perovskite structure type. In addition, CsPbBr₃ has already been shown to detect Ag x rays [14,15]. Since these compounds are being considered as hard radiation detector materials, a number of relevant properties such as defect stability need to be understood. Even very low concentrations of native defects and impurities can serve as traps and recombination centers that degrade the detector

performance [17]. Trapping of photoexcited carriers at defects decreases spectral resolution. Furthermore, surface recombination of carriers decreases the charge collection efficiency. The $\mu\tau$ value of a material is degraded by defect concentrations as low as a few ppm or even lower. Most chemically specific measurement techniques do not have the requisite sensitivity to detect defects at these low levels. In addition, they cannot detect native defects such as vacancies and antisite defects which can also result in decreased $\mu\tau$ values and detector efficiency. However, since many of these point defects are luminescent they can be detected by photoluminescence (PL) spectroscopy. Substitutional chemical impurities and native defects such as vacancies can manifest themselves as peaks in a PL spectrum, even at concentrations in the parts per billion range.

There are several prior PL studies of single-crystal CsPbX_3 compounds [3,5,14,15,19–21]. PL measurements on single-crystal samples of CsPbBr_3 have shown the presence of emission bands at 2.32 eV at temperatures up to 110 K that have been attributed to recombination of free excitons [3,5,14,15,19]. At 4.2 K, this peak is accompanied by several phonon replicas [3,19]. If this emission is indeed due to the free exciton it suggests that the compounds are nominally chemically pure and stoichiometric. However, a subsequent study of PL of single crystals of CsPbBr_3 grown by Bridgman revealed the presence of a broad peak below the band edge at 2.16 eV from 6 K up to 90 K [5]. This was attributed to emission from a defect or series of defect states, whose nature was not further investigated [5]. Previous PL measurements on single-crystal CsPbCl_3 indicated the presence of a free exciton peak at 2.98 eV, with additional peaks reported at 2.97, 2.96, and 2.94 eV [3]. The peak at 2.97 eV was tentatively attributed to either a bound exciton or band-edge luminescence, the peak at 2.96 eV to a phonon replica of the free exciton peak, and the peak at 2.94 eV was defect related, possibly a bound exciton.

Here we report on temperature- and power-dependent PL measurements of undoped CsPbX_3 Bridgman-grown single crystals. Thermal quenching measurements enable determination of the activation energies of the luminescent defects [22,23]. Power-dependent PL measurements are used to determine the defect species involved in radiative recombination: excitonic, donor-acceptor pair (DAP), or free-to-bound excitonic transitions [22,24]. For CsPbBr_3 , luminescence emission is observed at 2.33 and 2.29 eV at 10 K, persisting up to room temperature. For CsPbCl_3 , an excitonic peak is observed at 2.98 eV, along with additional peaks at 2.94, 2.96, and 2.97 eV. In both compounds the luminescence emission is above the conduction-band edge and is tentatively attributed to recombination involving halogen vacancy defect centers. Neither shallow nor deep level radiative defects are observed within the gap in these CsPbX_3 compounds.

II. EXPERIMENT

Single-crystal ingots of the compounds were grown by the vertical Bridgman method using a four-zone furnace with the temperature in the two top zones set to 700 °C and the two lower zones operating at 300 °C. The CsPbBr_3 samples reported in this study were synthesized as follows: PbBr_2 is dissolved in 48% aqueous HBr and added slowly, under

constant stirring at the initial steps, to a solution of CsBr dissolved in water. The mixture is left to cool down to ambient temperature and immediately filtered through a fritted-dish funnel under vacuum. The solid is washed with 8% aqueous HBr followed by methanol and dried overnight. The solid is further dried in an oven at ~ 70 °C in air. CsPbCl_3 was prepared similarly, with Cs_2CO_3 dissolved in 37% aqueous HCl being slowly added to PbO dissolved in 37% aqueous HCl under constant stirring to form the compound. The resulting CsPbCl_3 is filtered and dried as described above and then washed with 6% aqueous HCl followed by methanol and left for overnight drying. The solid is further dried in an oven at ~ 70 °C in air. Further details of CsPbX_3 synthesis, growth, and processing are presented elsewhere [15]. Small crystals that were suitable for x-ray diffraction were readily obtained from the boule and mounted on a STOE II image plate single-crystal diffractometer. Powder x-ray diffraction measurements were performed using a silicon-calibrated CPS 120 INEL powder x-ray diffractometer (Cu $K\alpha$, 1.54056 Å; graphite monochromatized radiation) operating at 40 kV and 20 mA. The crystal structures of the compounds were solved and refined using the SHELXL-2013 suite [25], aided by special functions of the PLATON [26] and WINGX [27] program suites. The as-grown crystal is semi-insulating with a resistivity $\sim 10^{10}$ Ω cm [15].

For PL measurements, the 405-nm line from a cw semiconductor diode laser is the excitation source. For temperature-dependent PL measurements, the excitation intensity was kept constant at 31.6 mW for CsPbBr_3 and at 15.8 mW for CsPbCl_3 as this was found to give the maximum overall PL intensity at 10 K. For the power-dependent PL measurement, the same excitation source was used, with a series of neutral optical density filters employed to vary the incident laser power from 2.0 to up to 50 mW for CsPbCl_3 and from 2.0 to up to 91 mW for CsPbBr_3 . An optical chopper and lock-in amplifier were used to improve signal to noise ratio. The PL emission spectra were resolved through the 0.75-m SPEX grating monochromator and detected by a Hamamatsu photomultiplier tube (R928). The sample was cooled to 10 K using a closed-cycle He cryostat (SHI Cryogenics DE-202).

First-principles calculations were performed in order to determine thermodynamic properties of intrinsic defects for the case of CsPbBr_3 . The projector augmented wave method [28] was implemented in the VASP code [29]. The generalized gradient approximation (GGA) method within the Perdew-Burke-Ernzerhof formalism [30] was employed for the exchange correlation functional, and the Heyd-Scuseria-Ernzerhof hybrid functional [31] was used to correct the band gap underestimation of the semilocal functional. The formation energy of defect D in charge state q ($\Delta H_{D,q}$) was calculated with the following formula:

$$\Delta H_{D,q} = E(D^q) - E(\text{Bulk}) - \sum_i n_i \mu_i + q E_F + E_{\text{corr}}, \quad (1)$$

where E is the total energy of a bulk or a defect system in a charge state q , n_i is a number of the atom i which is removed ($n < 0$) or added ($n > 0$) to form defect D , μ_i is the corresponding chemical potential of the element i , and E_F is the Fermi level [32]. Chemical potential μ_i is

determined with a growth condition and Fermi level E_F is determined self-consistently within the charge neutrality condition under the given growth temperature (T_g). E_{corr} is a correction term including the finite cell correction [33] and band-gap correction [34]. The defect level was determined with the charge transition level from q to $q'\varepsilon(q/q')$ defined by

$$\varepsilon(q/q') = [\Delta H_D(D, q) - \Delta H_D(D, q')]/(q' - q). \quad (2)$$

To describe isolated defect configurations, a $2 \times 2 \times 2$ supercell which accommodates 160 atoms was used. A $3 \times 3 \times 3$ k -point mesh was used for momentum space integration.

III. RESULTS AND DISCUSSION

A. Temperature-dependent PL studies

The PL spectra of CsPbBr₃ from 10 to 180 K are shown in Fig. 1(a). Scans from 2.2 to 2.5 eV show a single narrow emission peak centered at ~ 2.32 eV. The inset of Fig. 1(a) shows the decomposition of the spectrum at 10 K, where two peaks (at 2.33 and 2.29 eV) are observed using a Gaussian decomposition. The luminescence spectrum of CsPbBr₃ over a wide sub-band-gap energy range and increased sensitivity is shown in Fig. 1(c). The semilog plot indicates that no significant concentration of deep level defects exists in the compound. The peak centered at 2.33 eV has been previously assigned to a free exciton peak emission [3,5,19], while the peak located at 2.29 eV has been previously attributed to either a phonon replica of the free exciton [3] or to recombination involving a bound exciton state [5]. Absorption spectra obtained from a polished single crystal of CsPbBr₃ using UV-vis-IR transmission measurements as well as from a powdered CsPbBr₃ sample using diffuse reflectance [Fig. 2(a)] indicate that the room-temperature band gap for CsPbBr₃ crystal is ~ 2.23 eV. This value is in agreement with that previously reported [14,15]. As can be seen from Fig. 2(a), the absorption edge does not match the energy of the room-temperature PL emission. Thus it is concluded that the observed excitonic emission in these compounds is not due to band-to-band recombination as previously reported. This suggests that the luminescence involves a level above the conduction-band edge. We also note that the powder absorption spectra of both CsPbX₃ samples [Figs. 2(a) and 2(b)] reveal a feature above the band edge that roughly aligns with the emission peak position. However, the origin of this absorption feature is currently unknown.

The origin of the above-band-gap luminescence in CsPbBr₃ was investigated using density functional theory (DFT) calculations to determine the electronic states of defects. States ~ 0.23 and ~ 0.24 eV above the conduction-band edge due to Br vacancies are predicted. These calculations indicate that a recombination via bound excitons exists that should result in PL peaks with energies of ~ 2.46 and ~ 2.47 eV, respectively. These calculations of defect levels are in reasonable agreement with earlier DFT calculations on this compound by Shi and Du [35] which indicated a Br vacancy located at 0.16 eV above the conduction-band minimum. The observed room-temperature PL peak located at ~ 2.38 eV (~ 0.16 eV above the band gap) is thus tentatively attributed to recombination via a bound exciton involving a Br vacancy defect. In the observed luminescence, electrons are trapped by the Br vacancy defect

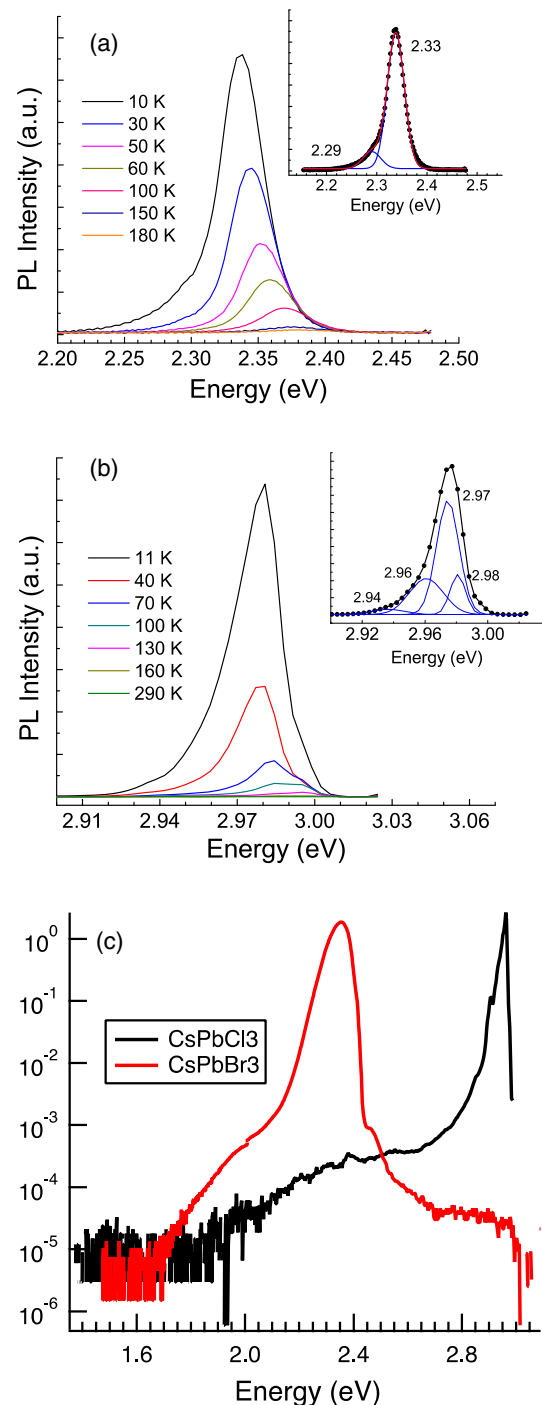


FIG. 1. (Color online) (a) PL spectra of CsPbBr₃ from 10 to 180 K. (inset) Two peaks are observed at 10 K, at 2.29 and 2.33 eV. (b) Spectra of CsPbCl₃ from 11 to 290 K. Inset: At 11 K (shown) and up to 100 K, four peaks are seen: 2.94, 2.96, 2.97, and 2.98 eV. Above 100 K, and up to 290 K all peaks except that at 2.94 eV are seen. (c) Semilog plots of the PL spectra of CsPbBr₃ and CsPbCl₃ over a wide sub-band-gap energy range and increased sensitivity.

and form a bound exciton with free holes in the valence band. Recently, such above-band-gap PL emission at room temperature in organo-lead halide perovskite CH₃NH₃PbI₃ was observed but in that case it was attributed to free carrier generation through rapid exciton dissociation [36]. While not

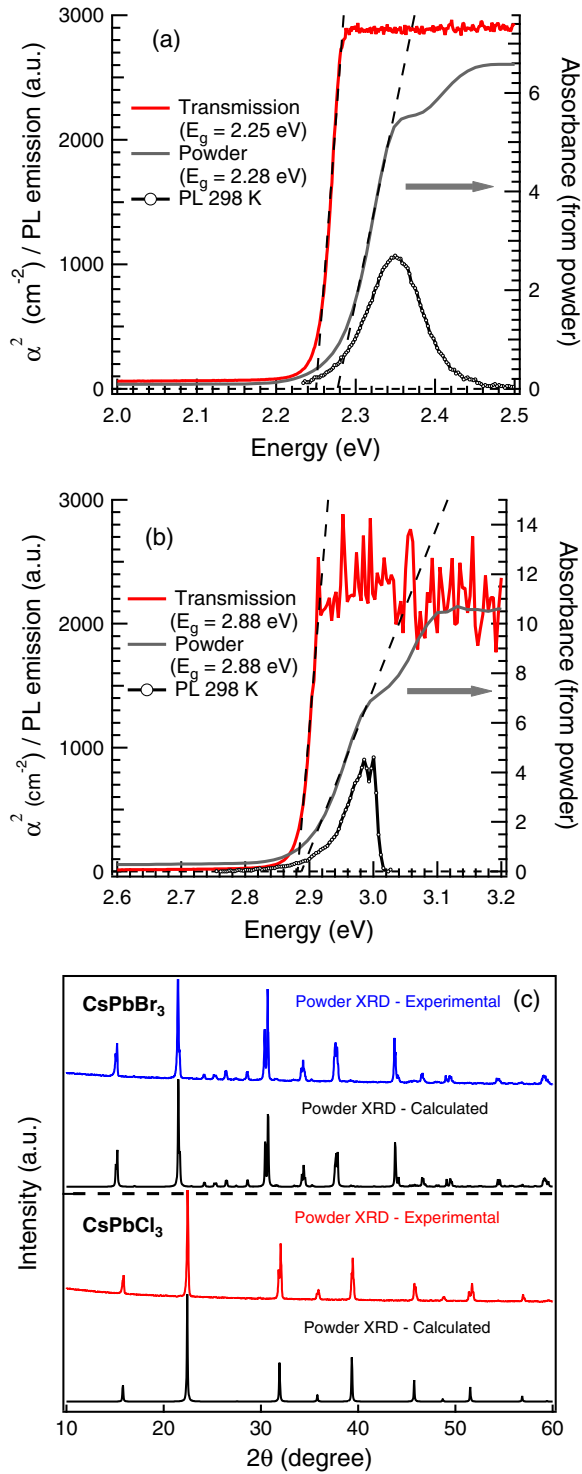


FIG. 2. (Color online) Plots of α^2 vs energy of (a) CsPbBr₃ and (b) CsPbCl₃ single crystals, calculated from transmission measurements at room temperature. (c) Powder x-ray diffraction spectra of CsPbX₃ samples.

typical, above-band-gap PL has also been observed in dilute GaAs_{1-x}N_x alloys [37] and GaAs_{1-x}P_x [38]. For the case of GaAs_{1-x}P_x, the above-band-gap emission was ascribed to recombination involving isoelectronic N traps with levels above the conduction-band edge. In the case of GaAs_{1-x}N_x alloys, the above-band-gap emission, however, was attributed

to a collection of perturbed conduction-band states near the *L* point. In the present case, a physical model of the PL process for the 2.38 eV peak can be described as follows: incident photons are absorbed by promoting electrons from the valence band into higher-lying excited states in the conduction band. Upon relaxation, an electron is then captured/trapped at a localized Br vacancy defect with energy level degenerate with conduction-band states. This is followed by the captured electron combining with a free hole in the valence band to form a bound exciton.

PL studies of CsPbCl₃ in the 2.9–3.03 eV range reveal a narrow peak overlapped on a broad shoulder centered at ~ 2.97 eV [Fig. 1(b)]. The luminescence spectrum in a wide sub-band-gap energy range and increased sensitivity is shown on a semilog plot in Fig. 1(c). It is possible that an extremely weak broad subgap emission (~ 2.3 – 2.6 eV) is present in CsPbCl₃. However, it is 10^4 times weaker than the dominant peak and thus only an extremely low concentration of deep level defects exists in CsPbCl₃. Gaussian decomposition of the PL signals below 100 K reveals four peaks centered at 2.94, 2.96, 2.97, and 2.98 eV [Fig. 1(b) inset]. Above 100 K and up to 290 K, only the latter three peaks listed are observed. This is to be compared to the room-temperature band gap for CsPbCl₃ crystals which is 2.85 eV [Fig. 2(b)]. Thus all the PL emission peaks in Fig. 2(b) are above the band gap. The peak centered at 2.98 eV could presumably be attributed to an exciton bound to a higher-lying defect state within the conduction band such as in the case for CsPbBr₃, with phonon replicas centered at 2.96 and 2.94 eV. A peak at 2.97 eV in CsPbCl₃ was previously attributed to a bound exciton [3], which is likely the identity of the 2.97 eV peak in this study.

Another possible interpretation of the observed emission band at 2.98 eV is luminescence from larger bandgap nanocrystalline inclusions embedded in the monocrystalline matrix. Luminescence of CsPbCl₃ nanocrystals embedded in CsCl:Pb single crystals has been previously reported [39], where an above-band-gap peak at 2.98 eV was observed at 10 K. Similarly, CsPbBr₃-like quantum dots exhibit PL emission in the 2.34–2.48 eV range at 5 K, which is above the band-gap energy of CsPbBr₃ single crystals and more closely matches that of CsPbBr₃ thin films [6]. However, powder X-ray diffraction (pXRD) results in the present study, shown in Fig. 2(c), indicate that the crystals are phase pure and therefore it is unlikely that we have nanoprecipitates in our CsPbX₃ samples. Alternatively, the observed recombination in CsPbX₃ could be associated with a higher-lying conduction-band edge. Furthermore, DFT calculations in the present study indicate that there are several higher-lying conduction bands within 0.2–0.5 eV of the lowest-lying conduction-band edge.

All emission peaks of CsPbBr₃ and CsPbCl₃ blueshift with increasing temperature [Figs. 3(a) and 3(b), respectively]. This is unexpected since excitonic PL typically redshifts with increasing temperature due to band-gap shrinkage [40]. Although there have been reports of blueshifting of the absorption edge with increasing temperature in other Pb-based semiconductors [41], this behavior has not been reported for CsPbBr₃. However, in the case of CdMnTe crystals blueshifting of a Mn²⁺ emission peak with temperature above 60 K has been observed. The ~ 0.04 eV shift was attributed to a multiphonon-assisted step-up process [42]. In this process,

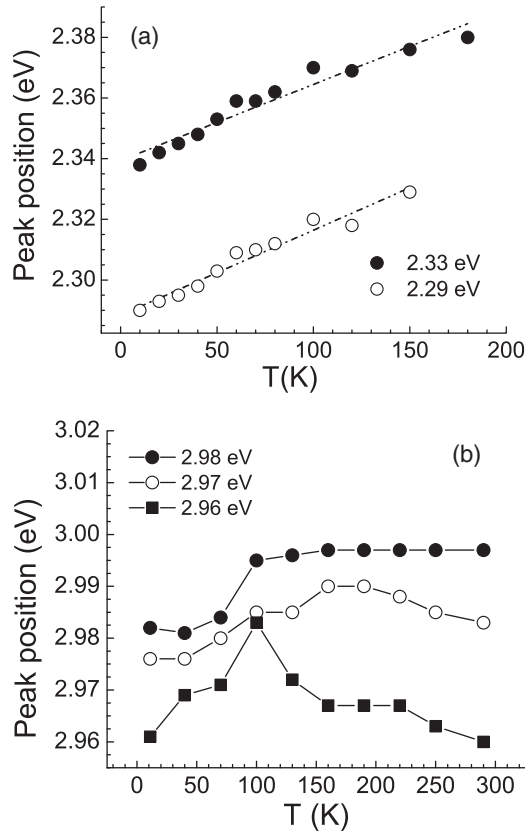


FIG. 3. (a) Peak position vs temperature, CsPbBr₃. The excitation intensity is 31.6 mW. The peak positions for both peaks are observed to blueshift with increasing temperature. (b) Peak position vs T , CsPbCl₃. The excitation intensity is 15.8 mW. The peak position is expected to continuously redshift as T increases, but this is only observed above ~ 150 K, and is not seen for the peak at 2.98 eV.

the carriers can reach a higher energy state due to phonon absorption, which is enhanced with increasing temperature. The observed blueshift of emission peaks with temperature in CsPbBr₃ by ~ 0.04 eV [Fig. 3(a)] is consistent with such a multiphonon process.

In the case of CsPbCl₃ the blueshift of the emission peaks is also unexpected [Fig. 3(b)]. The blueshift of the excitonic luminescence spectra has been previously observed in the 4.2–77 K range [20] and attributed to recombination involving a higher-energy radiative exciton state above the conduction-band edge. Furthermore a blueshift in the reflection spectra near the band edge was observed from 4.2 to 200 K indicating a widening of the band gap as temperature increases, with transitions possibly tracking with the band edge [20]. Therefore, the blueshift with increasing T for CsPbCl₃ below 100 K is attributed to the temperature-dependent band-gap widening. Above 100 K, however, the peak energies become invariant with temperature or redshift, although all peaks remain above the conduction-band edge [Fig. 3(b)].

To determine the phonon energy, E_{ph} , the line broadening of the band-edge PL emission for both compounds was measured as a function of temperature. The temperature dependence of peak width for excitonic peaks was analyzed using Toyozawa's

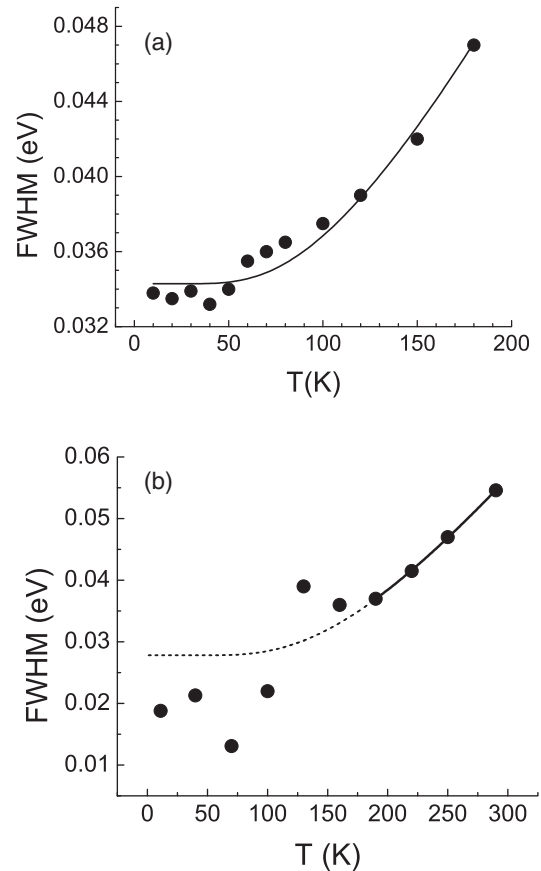


FIG. 4. (a) Peak FWHM vs T for CsPbBr₃. Fitting the data with Eq. (3) yields values of 0.016 eV E_{ph} . (b) Peak FWHM vs T , CsPbCl₃. Only the region from 190 to 300 K can be fitted with Eq. (3) since the material undergoes a phase transition at 185 K. The analysis yields values of 0.043 eV for E_{ph} .

equation [43,44],

$$\omega(T) = \frac{A}{\left[\exp\left(\frac{E_{\text{ph}}}{k_B T}\right) - 1\right]} + C, \quad (3)$$

where $\omega(T)$ is the peak full width at half maximum (FWHM) and C is a constant linewidth at low temperatures due to the absence of phonon broadening. From the analysis of spectral data shown in Fig. 4(a) using Eq. (3), a phonon energy E_{ph} of 0.016 eV was calculated for CsPbBr₃. This value is in good agreement with the value of a single-phonon energy of 0.016 eV [15] as well as 0.019 eV [3], previously obtained for this material using Raman spectroscopy.

Figure 4(b) shows the plot of $\omega(T)$ vs T for CsPbCl₃. The curve, however, is discontinuous at lower temperature and likely due to a reported phase transition at ~ 185 K [45]. The material is tetragonal based on our single-crystal refinement at room temperature and possibly over the whole 194–310 K range due to distortion of the perovskite structure. As a result of this structural phase change the data have only been fitted for the values from 185 to 295 K. A value of 0.043 eV is calculated for E_{ph} using Eq. (3). This value is in good agreement with a previously reported value of 0.046 eV for an LO phonon in CsPbCl₃ [46].

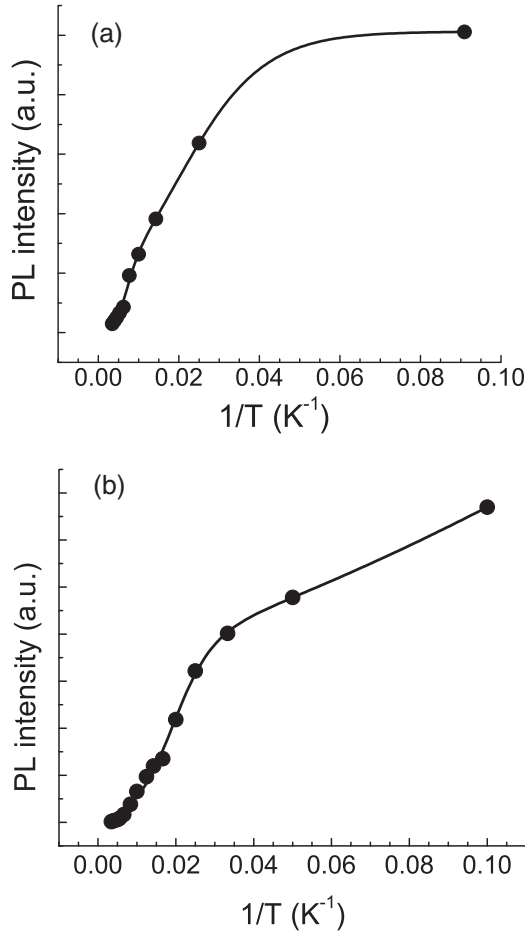


FIG. 5. (a) Peak intensity vs $1/T$, CsPbBr₃. Analysis of these data with Eq. (4) indicates that the high- and low-temperature activation energies are 0.017 and 0.0007 eV. (b) Peak intensity vs $1/T$, CsPbCl₃. Analysis of these data indicates that the high- and low-temperature activation energies are 0.057 and 0.0076 eV.

Thermal quenching of the PL intensity $I(T)$ can be analyzed using the two-step quenching model [47],

$$I(T) = \frac{I_0}{1 + C_1 \exp\left(-\frac{E_1}{k_B T}\right) + C_2 \exp\left(-\frac{E_2}{k_B T}\right)}, \quad (4)$$

where I_0 is the peak intensity at 0 K, E_1 and E_2 are the high- and low-temperature activation energies of nonradiative pathways, and C_1 and C_2 are related to the strength of the quenching processes. In the case of CsPbBr₃ the best fit analysis of the data in Fig. 5(a) to Eq. (4) yields values of 0.017 and 0.0007 eV for E_1 and E_2 , respectively. E_1 is often equated to the exciton binding energy [43,48] but in this case it is about half as much as that previously reported for this compound [3,19]. Furthermore the agreement between the values obtained from Eqs. (3) and (4) indicates that E_1 is the phonon energy.

For CsPbCl₃, values of 0.057 and 0.0076 eV for E_1 and E_2 , respectively, were obtained from the least-squares analysis of the data in Fig. 5(b) to Eq. (4). The value of E_1 is in excellent agreement with the value of 0.052 eV reported by Belikovich *et al.* for the activation energy of radiationless transitions in CsPbCl₃ [21]. CsPbX₃ compounds have previously been

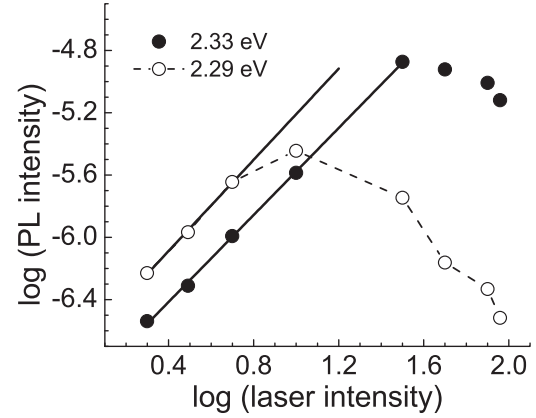


FIG. 6. A plot of $\log(\text{PL intensity})$ vs $\log(\text{incident laser intensity})$, CsPbBr₃. A linear fit of the low-excitation region (solid line) shows slopes of 1.5 and 1.4 for peaks centered at 2.29 and 2.33 eV, respectively. The PL intensity decreases, however, above an incident laser power of 10 mW for the shoulder peak, and 31.6 mW for the main peak.

reported to have large exciton binding energies, consistent with excitonic emissions persisting up to room temperature [3]. Their exciton binding energies are also consistent with those of semiconductors with similar band gaps [49].

B. Power-dependent PL studies

The nature of the recombination process can be determined from the dependence of the PL intensity on the excitation power [19]. It has been shown that the luminescence intensity I of the near-band-edge photoluminescence (NBEPL) emission lines is proportional to L^γ , where L is the power of the exciting laser radiation and the exponent γ is $1 < \gamma < 2$ for excitonlike transition and $\gamma < 1$ for free-to-bound and donor-acceptor pair (DAP) transitions [24]. All but one peak in the measured spectra have values of γ greater than 1 at low power (Figs. 6 and 7). This indicates that the recombination involves excitons. The exception is the 2.98 eV peak in CsPbCl₃ with a γ value of unity within error ($\gamma = 0.94 \pm 0.15$). The peak position, however, shows a blueshift as the excitation power is increased [Fig. 8(b)], which is not consistent with the behavior of a free-to-bound transition [50]. Thus it is concluded that the power-dependent PL measurements for CsPbX₃ indicate that all peaks are excitonic in nature.

The plot of integrated PL intensity vs laser power for CsPbBr₃ in Fig. 6 indicates that while the signals increase in intensity in the 0–10 mW range, a clear reduction in emission intensity is evident when the sample is irradiated with an intensity higher than 10 mW. This is unexpected since PL intensity should increase with increasing laser intensity. There are two possible mechanisms which can produce this effect. Due to our experimental conditions of high excitation power, this behavior could be attributed to carrier scattering effects. For a high concentration of photoexcited carriers, screening, scattering or self-annihilation of excitons occurs, decreasing the overall PL intensity at high excitation [51]. The other possibility is that PL fatigue is present in the material, characterized by a reduction in PL signal intensity as a function of time under prolonged light irradiation [49].

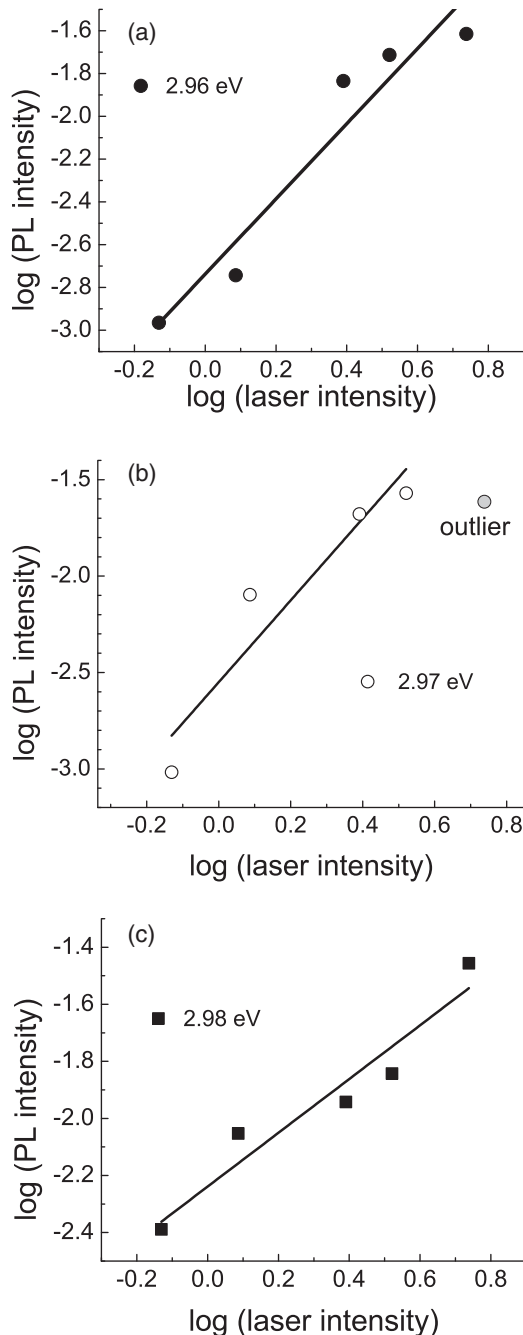


FIG. 7. log PL intensity vs log laser power for the three peaks seen at higher temperatures in CsPbCl₃. The laser intensity was varied from 2 to 50 mW. Linear fits are shown by the solid black lines. The γ values are 1.75 for (a), 1.57 for (b), and 0.94 for (c). These correspond to the peaks at 2.96, 2.97, and 2.98 eV, respectively.

Since the scans for each laser intensity level are done with only a few minutes between scans, it is possible that the material does not have time to equilibrate before being excited again. This PL fatigue has also previously been observed in other semiconductors including chalcogenide glasses [52], GaAs [53], and amorphous Si [54]. It should be noted, however, that PL fatigue has not been observed in CsPbBr₃ crystals and is currently under investigation to be presented elsewhere. The PL intensity reduction phenomenon was not

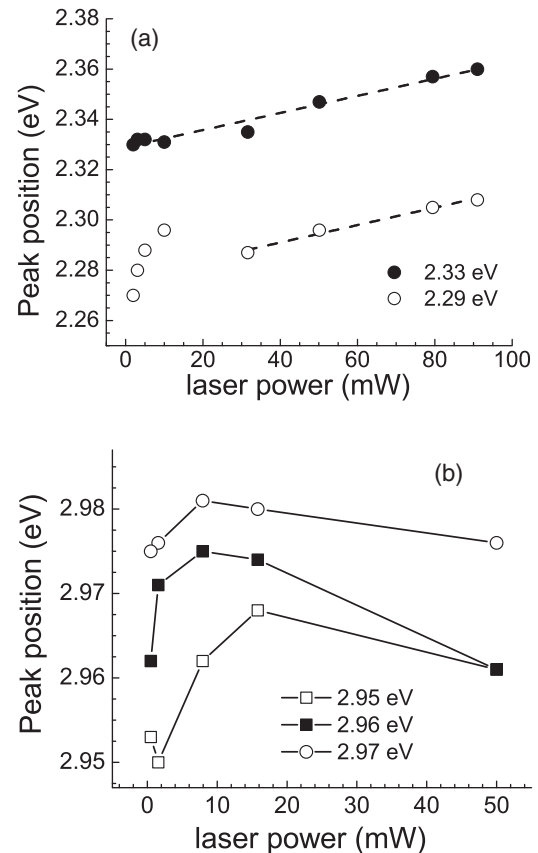


FIG. 8. (a) Peak position vs incident laser power for CsPbBr₃ at 10 K. (b) Peak position vs incident laser power for CsPbCl₃ at 10 K.

observed in CsPbCl₃ in this study, possibly due to the lower excitation power that was used.

C. DFT calculations

Calculations of the defect formation energy in CsPbBr₃ using density functional theory (DFT) indicate a series of defect levels attributed to native defects. In this study, we considered vacancies (V_{Cs} , V_{Pb} , V_{Br}) and antisite defects (Cs_{Pb} , Pb_{Cs} , Pb_{Br} , Br_{Pb} , Cs_{Br} , and Br_{Cs}). In Fig. 9(a), ΔH_D of V_{Cs} , V_{Pb} , V_{Br} , Cs_{Pb} , Pb_{Cs} , Br_{Cs} , and Br_{Pb} are presented as a function of the Fermi energy E_F for three different growth conditions (Cs-poor only, Br-poor only, and a combination of Cs and Br deficiencies). The formation energies (ΔH_D) of the antisite defects Pb_{Br} and Cs_{Br} are high and they are unlikely to be present. Calculations indicate that V_{Cs} , V_{Pb} , Cs_{Pb} , and Br_{Cs} have shallow acceptor levels (≤ 0.1 eV) and V_{Br} and Pb_{Cs} donor levels with relatively low defect formation energy, in agreement with recent DFT defect studies on CsPbBr₃ and other halide perovskites [35,55]. In contrast, Br_{Pb} has deep acceptor levels at 1.40 and 1.61 eV within the gap; however, its ΔH_D is high which again leads to a low concentration of this defect. Its maximum concentration under Cs-poor condition is 10^{13} cm⁻³ at 650 K.

The most dominant defects are then V_{Cs} , V_{Pb} , Pb_{Cs} , and V_{Br} . Of these, V_{Cs} and V_{Pb} result in shallow levels within the band gap, while V_{Br} and Pb_{Cs} have states ~ 0.23 and ~ 0.24 eV above the band gap. These values for V_{Br} are in

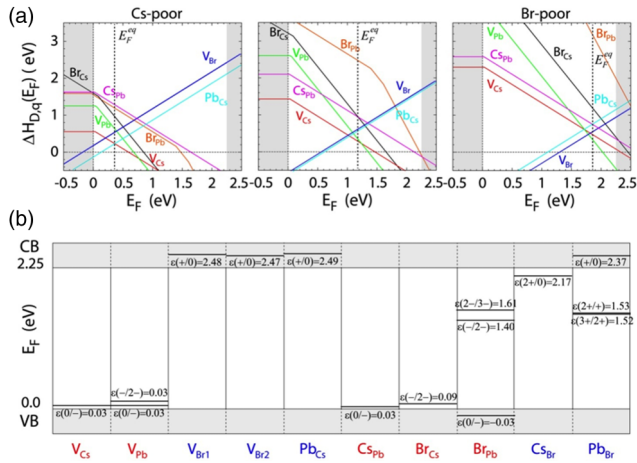


FIG. 9. (Color online) (a) Calculated defect formation energies in the $CsPbBr_3$ are plotted as a function of Fermi level. Left and right panels correspond to Cs-poor and Br-poor conditions, respectively. The middle panel is plotted for the midcondition between Cs-poor and Br-poor. Equilibrium Fermi level E_F^{eq} is plotted as black vertical dotted line. (b) Defect levels for vacancy and antisite defect of $CsPbBr_3$ are summarized. Defect levels are presented with respect to the valence band maximum. Blue and red text at the bottom of figure indicates acceptor and donor defects, respectively.

reasonable agreement with those recently reported by Shi and Du (0.16 eV, [35]) and support the experimental PL peak positions in the current study. Figure 9(b) summarizes calculated native defect levels of $CsPbBr_3$. It is worth noting here that our DFT calculations are still based on the GGA functional method and thus an accurate prediction of the enthalpies of formation (ΔH_f) is difficult. These calculations give indications concerning the nature of the defects but do not allow their unequivocal identification. Nevertheless, the fact that no significant concentration of stable charged defects

are observed in $CsPbBr_3$ indicates potentially excellent charge-transport properties in the form of high- $\mu\tau$ values for efficient charge collection in detector devices.

IV. CONCLUSION

Above band-gap luminescence in single-crystal perovskite compounds $CsPbX_3$ ($X = Cl, Br$) are observed. Power- and temperature-dependent photoluminescent properties are presented from 10 K up to 290 K. The power-dependent PL studies indicate that all peaks are excitonic involving bound excitons for both compounds. Both compounds exhibit above-band-gap luminescence which blueshifts with increasing temperature. $CsPbBr_3$ luminescence shows evidence of a resonant state located 0.16 eV above the conduction-band minimum, corresponding to the peak energy seen in the PL. This energy level is attributed to a Br vacancy on the basis of DFT calculations, which give indications concerning the nature of the defects. In both $CsPbBr_3$ and $CsPbCl_3$ all emission peaks undergo a blueshift with increasing temperature. For $CsPbBr_3$, phonon-assisted processes are responsible for the blueshift, while in $CsPbCl_3$ the blueshift is attributed to a widening of the band gap. No significant deep level or DAP luminescent peaks are observed in the PL spectrum of the $CsPbX_3$ perovskite compounds. The results indicate that these Bridgman-grown materials may be suitable for hard radiation detector applications due to the absence of radiative deep level defects that can serve as trapping centers.

ACKNOWLEDGMENTS

This work is supported by the U.S. Department of Energy National Nuclear Security Administration under Contract No. DE-AC02-06CH11357. The DFT calculations was supported by the Department of Homeland Security with Grant No. 2010-DN-077-ARI042-02. The authors thank Kyle McCall for technical assistance.

- [1] C. K. Moller, *Nature* **182**, 1436 (1958).
- [2] C. K. Moller, *Mat.-Fys. Medd.-Dan. Vidensk. Selsk.* **32**(1), (1959); **32**(2), (1959).
- [3] I. P. Pashuk, N. S. Pidzyrailo, and M. G. Matsko, *Sov. Phys. Solid State* **23**, 1263 (1981).
- [4] S. J. Clark, J. D. Donaldson, and J. A. Harvey, *J. Mater. Chem.* **5**, 1813 (1995); F. Somma, M. Nikl, K. Nitsch, P. Fabeni, and G. P. Pazzi, *J. Lumin.* **94-95**, 169 (2001); T. Sakuma, M. Mutou, K. Ohki, M. Arai, H. Takahashi, and Y. Ishii, *Solid State Ionics* **154-155**, 237 (2002); S.-i. Kondo, M. Kakuchi, A. Masaki, and T. Saito, *J. Phys. Soc. Jpn.* **72**, 1789 (2003); S. Kondo, K. Suzuki, T. Saito, H. Asada, and H. Nakagawa, *Phys. Rev. B* **70**, 205322 (2004); S. Kondo, K. Takahashi, T. Nakanish, T. Saito, H. Asada, and H. Nakagawa, *Curr. Appl. Phys.* **7**, 1 (2007).
- [5] K. Nitsch, V. Hamplová, M. Nikl, K. Polák, and M. Rodová, *Chem. Phys. Lett.* **258**, 518 (1996); C. C. Stoumpos and M. G. Kanatzidis, *Acc. Chem. Res.* **48**, 2791 (2015).
- [6] M. Nikl, K. Nitsch, E. Mihóková, K. Polák, P. Fabeni, G. P. Pazzi, M. Gurioli, S. Santucci, R. Phani, A. Scacco, and F. Somma, *Phys. E (Amsterdam, Neth.)* **4**, 323 (1999).
- [7] Y. H. Chang, C. H. Park, and K. Matsuishi, *J. Korean Phys. Soc.* **44**, 889 (2004); G. Murtaza and I. Ahmad, *Phys. B (Amsterdam, Neth.)* **406**, 3222 (2011).
- [8] M. Natarajan and B. Prakash, *Phys. Status Solidi (a)* **4**, K167 (1971); M. I. Cohen, K. F. Young, T. T. Chang, and W. S. Brower, *J. Appl. Phys.* **42**, 5267 (1971); S. Hirotsu, J. Harada, M. Iizumi, and K. Gesi, *J. Phys. Soc. Jpn.* **37**, 1393 (1974); J. Hutton, R. J. Nelmes, G. M. Meyer, and V. R. Eiriksson, *J. Phys. C: Solid State Physics* **12**, 5393 (1979); M. Sakata, T. Nishiwaki, and J. Harada, *J. Phys. Soc. Jpn.* **47**, 232 (1979); M. Sakata, J. Harada, M. J. Cooper, and K. D. Rouse, *Acta Crystallogr., Sect. A: Cryst. Phys., Diffr., Theor. Gen. Crystallogr.* **36**, 7 (1980).
- [9] A. Kojima, K. Teshima, Y. Shirai, and T. Miyasaka, *J. Am. Chem. Soc.* **131**, 6050 (2009).
- [10] I. Chung, B. Lee, J. He, R. P. H. Chang, and M. G. Kanatzidis, *Nature* **485**, 486 (2012).
- [11] L. Etgar, P. Gao, Z. Xue, Q. Peng, A. K. Chandiran, B. Liu, M. K. Nazeeruddin, and M. Grätzel, *J. Am. Chem. Soc.* **134**, 17396 (2012); H.-S. Kim, C.-R. Lee, J.-H. Im, K.-B. Lee, T. Moehl, A. Marchioro, S.-J. Moon, R. Humphry-Baker, J.-H.

- Yum, J. E. Moser, M. Grätzel, and N.-G. Park, *Sci. Rep.* **2**, 591 (2012); M. M. Lee, J. Teuscher, T. Miyasaka, T. N. Murakami, and H. J. Snaith, *Science* **338**, 643 (2012).
- [12] H. Zhou, Q. Chen, G. Li, S. Luo, T.-b. Song, H.-S. Duan, Z. Hong, J. You, Y. Liu, and Y. Yang, *Science* **345**, 542 (2014).
- [13] O. Busmundrud and J. Feder, *Solid State Commun.* **9**, 1575 (1971); J. Mizusaki, K. Arai, and K. Fueki, *Solid State Ionics* **11**, 203 (1983); R. L. Narayan, M. V. S. Sarma, and S. V. Suryanarayana, *J. Mater. Sci. Lett.* **6**, 93 (1987).
- [14] Z. Liu, J. A. Peters, C. C. Stoumpos, M. Sebastian, B. W. Wessels, J. Im, A. J. Freeman, and M. G. Kanatzidis, *Proc. SPIE* **8852**, 88520A (2013).
- [15] C. C. Stoumpos, C. D. Malliakas, J. A. Peters, Z. Liu, M. Sebastian, J. Im, T. C. Chasapis, A. C. Wibowo, D. Y. Chung, A. J. Freeman, B. W. Wessels, and M. G. Kanatzidis, *Cryst. Growth Des.* **13**, 2722 (2013).
- [16] S. Wang, Z. Liu, J. A. Peters, M. Sebastian, S. L. Nguyen, C. D. Malliakas, C. C. Stoumpos, J. Im, A. J. Freeman, B. W. Wessels, and M. G. Kanatzidis, *Cryst. Growth Des.* **14**, 2401 (2014).
- [17] A. Owens, *Compound Semiconductor Radiation Detectors* (CRC Press, Taylor & Francis Group, Boca Raton, FL, 2012).
- [18] K. Hitomi, Y. Kikuchi, T. Shoji, and K. Ishii, *IEEE Trans. Nucl. Sci.* **56**, 1859 (2009).
- [19] D. Fröhlich, K. Heidrich, H. Künzel, G. Trendel, and J. Treusch, *J. Lumin.* **18-19**, 385 (1979).
- [20] L. N. Amitin, A. T. Anistratov, and A. I. Kuznetsov, *Fiz. Tverd. Tela (Leningrad)* **21**, 3535 (1979) [*Sov. Phys. Solid State* **21**, 2041 (1979)].
- [21] B. A. Belikovitch, I. P. Pashchuk, and N. S. Pidzyrailo, *Optics Spectrosc.* **42**, 62 (1977).
- [22] K. Goksen, N. M. Gasanly, and R. Turan, *Cryst. Res. Technol.* **41**, 822 (2006).
- [23] J. Krustok, H. Collan, and K. Hjelt, *J Appl. Phys.* **81**, 1442 (1997).
- [24] T. Schmidt, K. Lischka, and W. Zulehner, *Phys. Rev. B* **45**, 8989 (1992); A. Bauknecht, S. Siebentritt, J. Albert, and M. C. Lux-Steiner, *J. Appl. Phys.* **89**, 4391 (2001).
- [25] G. M. Sheldrick, *Acta Crystallogr. Sect. A: Found. Crystallogr.* **64**, 112 (2008).
- [26] A. L. Spek, *Acta Crystallogr., Sect. D: Biol. Crystallogr.* **65**, 148 (2009).
- [27] L. Farrugia, *J. Appl. Crystallogr.* **45**, 849 (2012).
- [28] P. E. Blöchl, *Phys. Rev. B* **50**, 17953 (1994).
- [29] G. Kresse and J. Hafner, *Phys. Rev. B* **47**, 558 (1993); G. Kresse and J. Furthmüller, *ibid.* **54**, 11169 (1996).
- [30] J. P. Perdew, K. Burke, and M. Ernzerhof, *Phys. Rev. Lett.* **77**, 3865 (1996).
- [31] J. Heyd, G. E. Scuseria, and M. Ernzerhof, *J. Chem. Phys.* **118**, 8207 (2003); **124**, 219906 (2006).
- [32] C. Freysoldt, B. Grabowski, T. Hickel, J. Neugebauer, G. Kresse, A. Janotti, and C. G. Van de Walle, *Rev. Mod. Phys.* **86**, 253 (2014).
- [33] S. Lany and A. Zunger, *Phys. Rev. B* **78**, 235104 (2008).
- [34] D. Åberg, P. Erhart, A. J. Williamson, and V. Lordi, *Phys. Rev. B* **77**, 165206 (2008).
- [35] H. Shi and M.-H. Du, *Phys. Rev. B* **90**, 174103 (2014).
- [36] Q. Dong, Y. Fang, Y. Shao, P. Mulligan, J. Qiu, L. Cao, and J. Huang, *Science* **347**, 967 (2015).
- [37] P. H. Tan, X. D. Luo, Z. Y. Xu, Y. Zhang, A. Mascarenhas, H. P. Xin, C. W. Tu, and W. K. Ge, *Phys. Rev. B* **73**, 205205 (2006).
- [38] D. R. Scifres, N. Holonyak, C. B. Duke, G. G. Kleiman, A. B. Kunz, M. G. Craford, W. O. Groves, and A. H. Herzog, *Phys. Rev. Lett.* **27**, 191 (1971).
- [39] A. Voloshinovskii, S. Myagkota, A. Gloskovskii, and S. Zazubovich, *Phys. Status Solidi* **225**, 257 (2001).
- [40] P. Lautenschlager, P. B. Allen, and M. Cardona, *Phys. Rev. B* **31**, 2163 (1985).
- [41] V. D'Innocenzo, G. Grancini, M. J. P. Alcocer, A. R. S. Kandada, S. D. Stranks, M. M. Lee, G. Lanzani, H. J. Snaith, and A. Petrozza, *Nat. Commun.* **5**, 3586 (2014); N. Ashcroft and N. D. Mermin, *Solid State Physics* (Saunders College, Philadelphia, 1976).
- [42] H. Younghun, U. Youngho, and P. Hyoyeol, *J Korean Phys. Soc.* **58**, 1312 (2011).
- [43] C. J. Youn, T. S. Jeong, M. S. Han, and J. H. Kim, *J. Cryst. Growth* **261**, 526 (2004).
- [44] Y. Toyozawa, *Prog. Theor. Phys.* **27**, 89 (1962).
- [45] K. Wu, A. Bera, C. Ma, Y. Du, Y. Yang, L. Li, and T. Wu, *Phys. Chem. Chem. Phys.* **16**, 22476 (2014).
- [46] D. M. Calistru, L. Mihut, S. Lefrant, and I. Baltog, *J. Appl. Phys.* **82**, 5391 (1997).
- [47] D. Bimberg, M. Sondergeld, and E. Grobe, *Phys Rev. B* **4**, 3451 (1971).
- [48] E. Cohen, R. A. Street, and A. Muranovich, *Phys. Rev. B* **28**, 7115 (1983).
- [49] I. Pelant and J. Valenta, *Luminescence Spectroscopy of Semiconductors* (Oxford University Press, New York, 2012).
- [50] S. Levchenko, V. E. Tezlevan, E. Arushanov, S. Schorr, and T. Unold, *Phys. Rev. B* **86**, 045206 (2012).
- [51] D. C. Reynolds, D. C. Look, and B. Jogai, *J. Appl. Phys.* **88**, 5760 (2000); T.-R. Park, *J. Korean Phys. Soc.* **44**, 930 (2004).
- [52] T. Nakanishi, Y. Tomii, and K. Hachiya, *Electrochim. Acta* **100**, 304 (2013); *J. Non-Cryst. Solids* **354**, 1627 (2008); M. Seki and K. Hachiya, *J. Phys.: Condens. Matter* **15**, 4555 (2003).
- [53] D. Redfield and R. H. Bube, *Photoinduced Defects in Semiconductors* (Cambridge University Press, Cambridge, 1996).
- [54] I. Hirabayashi, K. Morigaki, and S. Nitta, *Jpn. J. Appl. Phys.* **19**, L357 (1980); D. Redfield and R. H. Bube, *Appl. Phys. Lett.* **54**, 1037 (1989).
- [55] W.-J. Yin, T. Shi, and Y. Yan, *Appl. Phys. Lett.* **104**, 063903 (2014).